DOI: 10.1002/ejic.200501020

Fe_3GeTe_2 and Ni_3GeTe_2 – Two New Layered Transition-Metal Compounds: Crystal Structures, HRTEM Investigations, and Magnetic and Electrical Properties

Hans-Jörg Deiseroth,*[a] Krasimir Aleksandrov,[a] Christof Reiner,[a] Lorenz Kienle,[b] and Reinhard K. Kremer[b]

Dedicated to Prof. Dr. Hanskarl Müller-Buschbaum on the occasion of his 75th birthday

Keywords: Layered compounds / Crystal structures / Iron germanium telluride / Magnetism / Electron microscopy / Conductivity

Fe_3GeTe_2 and Ni_3GeTe_2 are two new air-stable, black-metallic solids. They were characterized by single-crystal X-ray crystallography, high resolution transmission electron microscopy (HRTEM), and preliminary magnetic measurements. Both compounds crystallize in the hexagonal system [$P6_3/mmc$, $Z = 2$; Fe_3GeTe_2: $a = 399.1(1)$ pm, $c = 1633(3)$ pm; Ni_3GeTe_2: $a = 391.1(1)$ pm, $c = 1602.0(3)$ pm], and represent a new structure type with a pronounced macroscopic and microscopic layer character. They show close structural relationships to iron/nickel germanium alloys. Each layer in the title compounds represents a sandwich structure with two layers of tellurium atoms covering a triple-layer Fe_3Ge (Ni_3Ge) substructure on both sides. Assuming full occupancies for the Fe and Ni sites, a mixed-valence formulation for the transition-metal atoms according to $(M^{2+})(M^{3+})_2(Ge^{4-})(Te^{2-})_2$ (M = Fe, Ni) may be concluded. A slightly reduced occupancy for one Fe/Ni position, however, indicates a more complicated local structural situation. This is confirmed by weak residual electron density in the van der Waals gap and by the results of detailed HRTEM and electron-diffraction experiments for Ni_3GeTe_2. The latter results show variations in the arrangement of Ni atoms, as well as vacancies and a misfit of in-plane disordered hexagonal layers. Fe_3GeTe_2 shows Curie–Weiss behavior above and ferromagnetism below 230 K, while Ni_3GeTe_2 exhibits temperature-independent paramagnetism in the measured temperature range and a metallic behavior of the electrical resistance.

Introduction

The title compounds represent two unexpected new solids. They were obtained from a series of experiments aimed at the syntheses of new mixed-valence compounds with *transition metals* related to those compounds with *main group elements* investigated in our group.[1,2]

Fe_3GeTe_2 is possibly identical to a solid obtained earlier[3] that could not, however, be structurally characterized. Ni_3GeTe_2 has not been reported previously. The crystal structures of both compounds exhibit a pronounced layer character with layered Fe_3Ge (Ni_3Ge) substructures sandwiched by two layers of Te atoms and a van der Waals gap between adjacent Te layers. The Fe_3Ge and Ni_3Ge substructures are closely related to layered sections of the structures of alloys with the compositions $Fe_{1.67}Ge$[4] and $Ni_{1.67}Ge$.[5] From a general topological viewpoint, a close relationship with respect to the sandwich character is also obvious to a group of layered metal-rich Nb, Ta, and Hf chalcogenides and to Pd_5AlI_2 characterized earlier by different authors.[6–9] The latter solid is the earliest example to fit into this group of unconventional layer structures. In all these solids, at least three layers of metal atoms (or mixed-metal and semimetal atoms) are sandwiched between two layers of chalcogen (or halogen) atoms.

For both compounds there seems to be a simple mixed-valence formulation like $M_3GeTe_2 = (M^{2+})(M^{3+})_2(Ge^{4-})(Te^{2-})_2$, which is strongly supported by the crystallographic multiplicity of the respective atomic sites. However, disorder phenomena and structural inhomogeneity, in combination with the general properties of the new solids, make a simple formulation as type 1 mixed-valence solids[10] with clearly distinguishable oxidation states most unlikely, and complicate a concise description of these new compounds.

[a] Anorganische Chemie, Universität Siegen,
Adolf-Reichwein-Straße, 57068 Siegen, Germany
Fax: +49-271-7402555
E-mail: deiseroth@chemie.uni-siegen.de
[b] Max-Planck-Institut für Festkörperforschung,
Heisenbergstraße 1, 70569 Stuttgart, Germany
Fax: +49-711-689-1091
E-mail: L.Kienle@fkf.mpg.de

Table 1. Summary of the data collection and refinement details for Fe_3GeTe_2 and Ni_3GeTe_2.

Name	Triiron germanide ditelluride	Trinickel germanide ditelluride
Chemical formula	Fe_3GeTe_2	Ni_3GeTe_2
Molecular mass [g/mol]	495.34	503.9
Temperature [K]	293(2)	293(2)
Wavelength [pm]	Mo-K_α, λ = 71.073	Mo-K_α, λ = 71.073
Crystal system, space group	hexagonal, $P6_3/mmc$ (No. 194)	hexagonal, $P6_3/mmc$ (No. 194)
Cell dimensions [pm]	a = 399.1(1), c = 1633(3)	a = 391.1(1), c = 1602.0(3)
Volume [10^6 pm^3]	225.34(9)	212.10(9)
Z, X-ray crystal density [g/cm^3]	2, 7.3	2, 7.89
Absorption coefficient [mm^{-1}]	28.552	33.389
F(000)	428	440
Diffractometer	IPDS (Stoe)	IPDS (Stoe)
Scan type	φ	φ
Crystal size [mm]	0.15×0.15×0.01	0.08×0.08×0.03
Measured range (θ) [°]	2.49–25.79	6.02–30.31
Index ranges	$-4 \le h \le 4$	$-4 \le h \le 5$
	$-4 \le k \le 4$	$-5 \le k \le 5$
	$-20 \le l \le 20$	$-22 \le l \le 17$
Measured reflections; unique; significant	1566; 113; 112	1182; 156; 120
R_{int}, R_σ	0.0535, 0.0225	0.0484, 0.0239
Completeness to (θ) [°]	93.8% (25.79)	91.1% (30.31)
$T_{min.}$, $T_{max.}$	0.0048, 0.5039	0.029, 0.073
Structure solution	direct methods[a]	direct methods[a]
Structure refinement	full-matrix least-squares on F^2 [b]	full-matrix least-squares on F^2 [b]
Data/restraints/parameter	113/0/15	156/0/16
$S(F_2)$	1.547	1.061
Absorption correction	numerical[c]	numerical[c]
R_1, wR_2 [$I > 2\sigma(I)$]	0.0328, 0.0731	0.0282, 0.0608
R_1, wR_2 (all data)	0.0330, 0.0731	0.0396, 0.0628
Extinction coefficient	0.069(7)	0.007(1)
ρ_{min}, ρ_{max}	–1.9(5), 1.6(5)	–1.5(4), 1.5(4)

[a] G. M. Sheldrick, SHELXS-97, Program for the Solution of Crystal Structures, University of Göttingen, 1997. [b] G. M. Sheldrick, SHELXL-97, Program for Structure Refinement, University of Göttingen, Germany, 1997. [c] STOE & CIE, X-SHAPE 1.06, Darmstadt, 1999.

Here we present information about the preparation conditions and the crystal structures obtained by X-ray single-crystal and powder diffraction studies. Detailed discussions of the real structure based on results from HRTEM and SAED (Selected Area Electron Diffraction) studies of Ni_3GeTe_2 are also provided. In addition, preliminary temperature-dependent measurements of the magnetic susceptibility for powder samples of both compounds are presented.

Results and Discussion

Tables 1, 2, and 3 contain the relevant crystallographic and crystal chemical results for the title compounds.

Table 2. Atomic coordinates, Wyckoff notations, site occupation factors, and equivalent isotropic displacement parameters U_{eq} [10^4 pm^2] for Fe_3GeTe_2 and Ni_3GeTe_2 (printed in *italics*). U_{eq} is defined as one-third of the trace of the orthogonalized U_{ij} tensor.

Atom	Wyckoff	x	y	z	U_{eq}	$s.o.f.$
Fe1	4e	0	0	0.6718(1)	0.0086(7)	1.0(1)
Ni1	*4e*	*0*	*0*	*0.6670(1)*	*0.0097(5)*	*1*
Fe2	2c	0.6667	0.3333	0.75	0.0077(2)	0.83(2)
Ni2	*2c*	*0.6667*	*0.3333*	*0.75*	*0.007(1)*	*0.70(1)*
Ni3	*2a*	*0*	*0*	*0.5*	*0.010(3)*	*0.25(1)*
Ge	2d	0.3333	0.6667	0.75	0.021(1)	0.99(2)
Ge	*2d*	*0.3333*	*0.6667*	*0.75*	*0.0218(6)*	*1*
Te	4f	0.6667	0.3333	0.59018(6)	0.0096(7)	1
Te	*4f*	*0.6667*	*0.3333*	*0.58852(6)*	*0.0079(4)*	*1*

Fe_3GeTe_2

Figure 1 shows a projection of the crystal structure of Fe_3GeTe_2, emphasizing that layers of Te atoms sandwich 2D structural sections built from Fe and Ge atoms. The shortest distance d(Te–Te) between adjacent layers amounts to 374 pm. In order to illustrate the Fe/Ge substructure in more detail, the three atomic layers consisting of Fe, Fe/Ge, and Fe atoms are projected along [001] in part b of Figure 1. A comparison with structural data given in the literature for $Fe_{1.67}Ge$ (see earlier) reveals that this alloy contains similar hexagonal layers of Fe and Fe/Ge atoms, however, it forms a compact, isotropic 3D structure without any macroscopic layer character. It should be noted that the chemical composition as obtained by refinement of the crystallographic occupational parameters based on single-crystal X-ray data gives $Fe_{2.83}GeTe_2$ instead of Fe_3GeTe_2 (Table 2). This minor but significant difference was repeatedly found for different crystals. It stems from an occupational deficiency of the Fe2 site (forming a common layer with Ge), however, it differs from results obtained by analytical scanning electron microscopy for a variety of crys-

Table 3. Selected interatomic distances *d* [pm] for Fe_3GeTe_2 and Ni_3GeTe_2.

		Fe_3GeTe_2	Ni_3GeTe_2
Ge	–Fe2/Ni2 (3×)	230.42(6)	225.74(6)
	–Fe1/Ni1 (6×)	263.4(1)	261.9(1)
Fe1/Ni1	–Fe1/Ni1	255.4(4)	265.6(4)
	–Fe2/Ni2 (3×)	263.4(1)	261.9(1)
	–Ge (3×)	263.4(1)	261.9(1)
	–Te (3×)	266.2(1)	258.5(1)
	–Ni3	–	267.7(2)
Fe2/Ni2	–Ge (3×)	230.42(6)	225.74(6)
	–Te (2×)	261.1(1)	266.59(7)
	–Fe1/Ni1 (6×)	263.4(1)	261.9(1)
Ni3	–Te (6×)	–	266.59(7)
	–Ni1 (2×)	–	267.7(2)

tals. These strongly support the composition Fe_3GeTe_2 for the series of tested crystals. A possible solution for this contradiction assumes a marginal fraction of 0.17 Fe atoms (per formula unit) statistically distributed over atomic positions in the van der Waals gap. This problem is even more pronounced for the corresponding Ni atoms in Ni_3GeTe_2, and is therefore discussed together with the character of the coordination polyhedra and further structural details later.

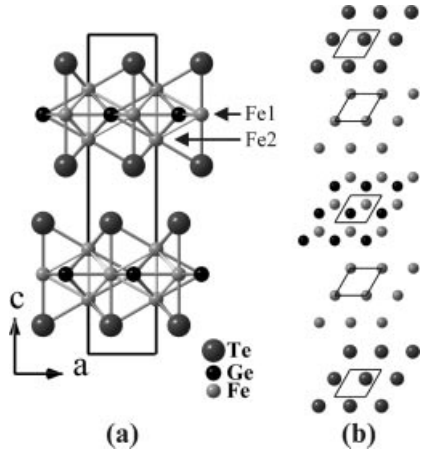

Figure 1. (a) Projection of the crystal structure of Fe_3GeTe_2 along [010]. (b) [001] projections of the single Te, Fe, and mixed Fe/Ge layers of the upper layer package.

Ni_3GeTe_2

Figure 2 (a) shows a projection of the crystal structure of Ni_3GeTe_2 along [010], which is basically isotypic to Fe_3GeTe_2. Even more pronounced than for Fe_3GeTe_2, a significant residual electron density in the van der Waals gap is observed in the refinement of the single-crystal X-ray diffraction data. The reliability factor of the refinement significantly improves if we assume partial occupancy (0.25) of the Ni3 site located in the van der Waals gap between adjacent Te layers.

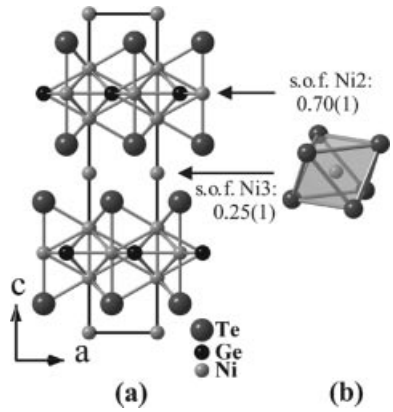

Figure 2. (a) Projection of the crystal structure of Ni_3GeTe_2 along [010]. (b) The octahedral coordination polyhedron for Ni3 (this Ni-position is located in the van der Waals gap with an approximate occupancy of 0.25).

In Figure 2 (b), the coordination polyhedron for Ni3 is displayed. It is similar to the coordination polyhedron found, for example, for Ni in $NiTe_2$ (CdI_2 type[11]). This Ni3–Te partial structure can be treated as a 2D section of a Ni-deficient $NiTe_2$ structure. Together with the reduced occupancy of Ni2 (Table 2), the occupancy of Ni3 completes the chemical composition to give $(Ni3)_{0.25}(Ni2)_{0.7}(Ni1)_2GeTe_2 = Ni_{2.95}GeTe_2$.

From the inspection of SEM images (Figure 3), it is most likely that the presence of Ni3 in the van der Waals gap causes a stronger cohesion between adjacent layers, and may be responsible for the more compact and less pronounced layer character of the Ni_3GeTe_2 sample in comparison with Fe_3GeTe_2.

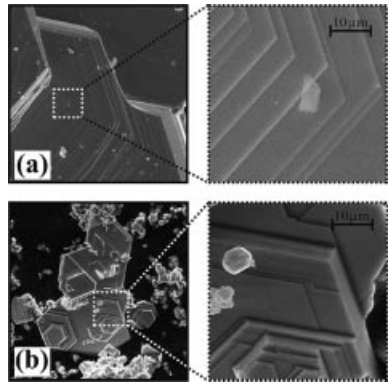

Figure 3. A comparison between SEM images of (a) Fe_3GeTe_2 and (b) Ni_3GeTe_2 showing the hexagonal platelets which are characteristic for both compounds. The platelets formed by the Ni compound are thicker and more compact.

Further Crystal Chemical Aspects

The individual coordination polyhedra shown in Figure 4 for Fe_3GeTe_2 clearly demonstrate that there is no typical coordination geometry (for example, tetrahedral) around the germanium atoms that would formally allow a +4 oxidation number to be ascribed to the Ge atoms. In-

stead, the germanium atoms are surrounded by iron atoms exclusively in their first coordination sphere, whereas tellurium atoms are typical constituents of the second coordination sphere [the shortest d(Ge–Te) = 348 pm in comparison with the shortest d(Ge–Fe) = 230 pm]. On the other hand, both types of iron atoms (Fe1 and Fe2) are coordinated by Ge, Fe, *and* Te atoms in their first coordination sphere (Figure 4), suggesting in particular significant Fe–Fe interactions [the shortest d(Fe–Fe) = 255 pm in comparison to d(Fe–Fe) = 250 pm in alpha-Fe]. At first glance, these structural details partly seem to support the earlier mentioned simple ionic description of Fe_3GeTe_2 as (Fe^{2+})-$(Fe^{3+})_2(Ge^{4-})(Te^{2-})_2$.

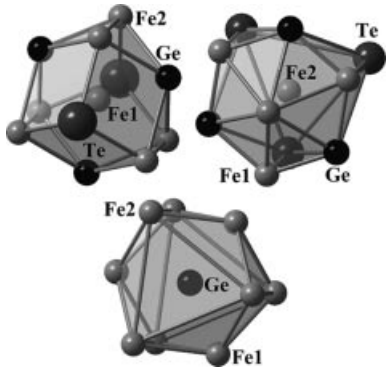

Figure 4. Coordination polyhedra around Fe1, Fe2, and Ge in Fe_3GeTe_2.

If we omit the enclosing Te atom layers and the Ni atoms located in the van der Waals gap, we can clearly see from Figure 5 that the Fe/Ge and Ni/Ge atoms form a 2D system of trigonal prisms $GeFe(2)_{6/3}$ interconnected by additional Fe(1) atoms, or alternatively as a system of trigonal prisms $Fe(1)Fe(2)_{6/3}$ interconnected by Ge atoms. The first view is reminiscent of the aspect that the 2D partial structure represented in this way can be interpreted as a stuffed 2D NiAs structure.

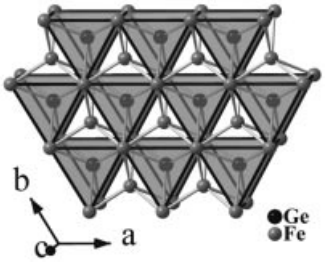

Figure 5. The 2D Fe_3Ge (Ni_3Ge) partial structure of Fe_3GeTe_2 (Ni_3GeTe_2) visualized as a 2D arrangement of trigonal prismatic $GeFe_{6/3}$ units interconnected by Fe atoms or as a 2D system of trigonal prismatic $FeFe_{6/3}$ units interconnected by Ge atoms.

A comparison of Fe_3GeTe_2 and Ni_3GeTe_2 based on the statements given earlier shows that the most important difference between their crystal structures concerns the partially occupied atomic position Ni3 (0.25 Ni per formula unit) located in the van der Waals gap. In the case of the iron compound this position does not show any significant residual electron density. A supporting argument comes from the experimental observation that $NiTe_2$ crystallizes in the CdI_2 structure type[12] with Ni in a similar coordination as Ni3 in Ni_3GeTe_2. $FeTe_2$ on the other hand does *not* crystallize in this structure type. Instead, only a marcasite modification of $FeTe_2$ is known.[12] Thus, the crystal structure of Ni_3GeTe_2 can actually be treated as an intergrowth species between the two Ni-deficient constituting phases Ni_xTe_2 and $Ni_{1-x}Ni_2GeTe_2$ with $x = 0.25$.

In order to clarify the structural situation, it must be mentioned at this point that a completely *ordered* distribution of Ni3 (hypothetical Fe3) would require multiple lengths of a and b (not c). A fully (or partially) *ordered* distribution of Ni3 on the other hand would result in additional (diffuse) superstructure reflections. It was found that more detailed information on this subtle problem could only be derived from HRTEM and SAED investigations with Ni_3GeTe_2 (see later), and not from the X-ray structure analyses.

HRTEM and SAED Investigations of Ni_3GeTe_2

Our study was specifically focused on the degree of structural disorder on the nanometer scale, and in particular on the examination of the Ni and Ge atomic disorder. Disorder phenomena resulting from X-ray analyses in many cases have been artificially generated by a superposition of ordered real structure components, like domains or stacks of layers with ordered structure. In fact, some peculiarities of the morphology could be addressed to layered components: see the well-defined microstructure in the bright field images of Figure 6 (part a, zone axis [001] and part b). Electron-diffraction patterns along zone axes [uv0] demonstrate that all stacks are strictly parallel to (001). Figure 6 (b) was recorded along zone axis [100], and hence displays the (001) stacks edge on. The lower limit of their thickness is in the range of several nanometers. The stacks separate at the outermost rims of the crystals, while they match perfectly at coherent boundaries in thicker areas. HRTEM proves that the stacks are not significantly shifted to each other; therefore, they are not part of a classical polytypic structure. EDX linescans indicate no noticeable changes in the average composition of adjacent stacks, particularly not of the Ni/Ge ratio. At first glance, SAED patterns (tilting experiments) are in good agreement with patterns simulated on the basis of the average structure. However, closer inspection reveals two kinds of intensities in addition to the main structure reflections. Both phenomena indicate marginal deviations of the real structure from the disordered average structure.

The first one includes weak diffuse rods parallel to [001]* intersecting all positions ${}^{h}/_{3}{}^{h}/_{3}0$ and ${}^{2h}/_{3}{}^{2h}/_{3}0$ of the reciprocal space which are equivalent for the hexagonal system. The rods are shown as diffuse lines in patterns containing [001]* (see for instance zone axis [210] in Figure 6, c), while they are cut into intersection points in [001] patterns (Figure 6, d). The diffuse intensity observed in different areas of the same crystallite is variable, as demonstrated by the

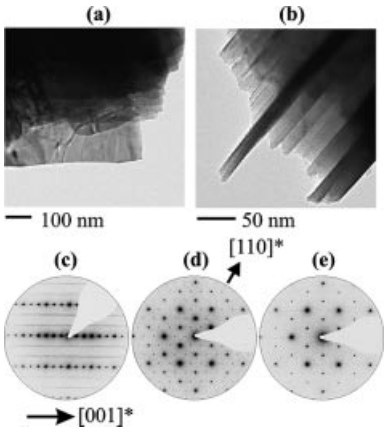

Figure 6. Bright field images of compact crystals, (a) zone axis [001] and (b) zone axis [100]. Electron-diffraction patterns with diffuse intensities, (c) for [210], and intersection points, (d) [001]. Pattern (e) was recorded on another selected area of the same crystal as (d).

existence or absence of intersection points, cf. Figure 6 (parts d and e). In some cases, we observed [001] patterns without any diffuse scattering in the precise zone axis orientation, however, when tilting the diffuse intensities became significant (see later).

Taking into account the high sensitivity of electron-diffraction experiments and the exceptionally weak diffuse intensity observed, the lack of such intensities in X-ray diffraction patterns can be rationalized. It was challenging to image the deviation from the average structure, especially because of the beam sensitivity of the sample under the conditions of HRTEM. However, with selection of low dose modes, we were at least able to record [001] micrographs with significant intersection points in the Fourier transforms. An interpretation of the scattering phenomena in real space is complicated as a result of moiré effects (see later). However, a basic interpretation is straightforward, that is, the existence of diffuse rods in reciprocal space correlates with the evolution of structural order within layers of direct space. For the modeling of such in-plane ordering, ordered arrangements of Ni atoms and vacancies in the Ni and (Ni, Ge) layers were introduced. Additionally, the occupancy factors were fixed to the average values. Prototypes for such ordering can be derived from the structures of (Ni, Ge) intermetallics. Those compounds show related disorder phenomena to those observed for Ni_3GeTe_2. A top view of a mixed (Ni, Ge) layer of Ni_5Ge_3[13] is characterized by an ordered vacancy distribution (see Figure 7).

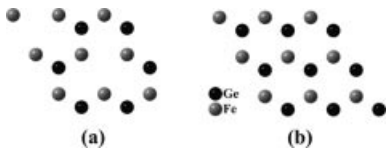

Figure 7. (a) Top view of the ordered (Ni, Ge) layer of Ni_5Ge_3. (b) Top view of the disordered (Ni, Ge) layer in Ni_3GeTe_2.

The composition of this layer is the same as that of the mixed and disordered (Ni2, Ge) layer in Ni_3GeTe_2. The ordered vacancies can be introduced in large supercells, which serve for simulation. The simulated [001] SAED pattern shows, like the experimental patterns, intensities in addition to the main structure reflections on all positions $^{h}/_{3}{}^{h}/_{3}0$ and $^{2h}/_{3}{}^{2h}/_{3}0$. The occurrence of diffuse scattering in the experimental patterns could be interconnected with a nonperiodic sequence of the ordered layers, for example by applying rotations of adjacent layers. In the case of disorder, the intensity distribution within the diffuse rods depends on the degree of structural order within the analyzed area. If the structure appears to be randomly arranged along [001], for instance by assuming equal numbers of ordered layers with 0°, ±60°, and ±120° rotation (rotation axis [001]), we expect no intersection points in the zero-order Laue zone of [001] patterns. However, diffuse intensity should be present in layers slightly above (001)*; hence, the formation of intersection points by tilting slightly from precise [001] zone axis orientation is rationalized. As shown by simulated micrographs, the significance of ordered vacancies in HRTEM micrographs is marginal, in particular for real structures containing a disorder of layers. Therefore, future projects are focusing on HRTEM on long-term annealed samples which may be long-range ordered crystals.

The second type of diffracted intensity, in addition to the main structure reflections, can be assigned to moiré effects based on a misfit of hexagonal layers (see later). In this case, no diffuse intensities were observed as evidence of an in-plane disordered arrangement of Ni atoms and vacancies. Along [001], the misfit produces characteristic patterns of double diffraction (see Figure 8).

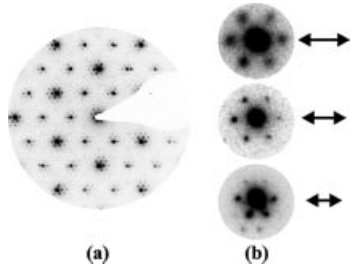

Figure 8. Double diffraction patterns in [001], (a) typical example and (b) enlarged sections of patterns, displaying distinct difference vectors (Δd, see arrows).

No multiple twinning (triplets) of stacks with a lower symmetry than hexagonal (for example, orthorhombic *C*) is shown. All [001] patterns as well as Fourier transforms of HRTEM images show perfect hexagonal symmetry and no splitting of the main structure reflections. As a rule, a translational moiré effect is observed, which is based on hexagonal layers with parallel orientation of all lattice vectors but with significant variations of the in-plane (*a*) lattice parameter. The changes of the lattice could be interconnected with strain, for example because of in-plane aggregation of Ni atoms on Ni2 and Ni3 positions within adjacent (001) stacks. The lattice mismatch varies from crystal to crystal: see the arrows in Figure 8 (b) which highlight the distinct

difference vectors of both lattices. Slight variations of the mismatch are also evident within the same crystallite. The in-plane aggregation could be interconnected with variations in the density of the Ni atoms in consecutive (001) layers containing Ni2 and Ni3 positions. To check for such real structures, the average density of the Ni atoms was split in terms of more or less occupied Ni2 and Ni3 positions within consecutive (001) layers. The significance of such separation in HRTEM micrographs is demonstrated for [100] in Figure 9 (a). The simulations were calculated close to Scherzer defocus. The black contrasts correspond to atoms (high projected potential), and the white contrasts correspond to cavities (low projected potential), with both superimposed in rows along [100]. The black and gray arrows highlight the layers containing Ni2 and Ni3 positions edge on. Starting from a ratio of occupied positions Ni2/Ni3 = 100:0, the average occupation of Ni2 layers was decreased while that of Ni3 was increased in steps of the same value. The series of simulations clearly demonstrates that the significance of HRTEM is limited to full separation which has never been experimentally observed, not even by selection of different focusing conditions (see Figure 9, b). On the contrary, all experimental images are in good agreement with the simulated images based on the average structure. The occupation of the position Ni3, for example, is in accordance to the average structure low, and a separation in layers with full and nonoccupied positions Ni3 can be excluded. Hence, the mismatch must be based on in-plane aggregations of Ni atoms without significant changes to the average occupancy factors.

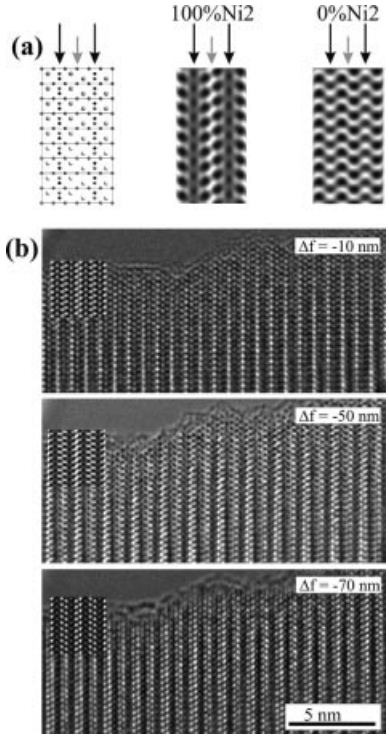

Figure 9. (a) Simulated micrographs for Scherzer defocus (zone axis [100]) with different densities on positions Ni2, Ni3; see text. (b) Defocus series with inserted simulations ([100], thickness: 3.2 nm).

To conclude, the ordering of Ni atoms and vacancies in the real structure is never complete. Two scattering phenomena demonstrate variations in the arrangement of Ni atoms and vacancies. The first one (diffuse intensities) indicates in-plane ordering, while the second one (double diffraction) is characterized by a misfit of in-plane disordered hexagonal layers.

Magnetism of Fe_3GeTe_2 and Ni_3GeTe_2 and Electrical Conductivity of Fe_3GeTe_2

Preliminary measurements of the temperature dependence of the magnetic susceptibility reveal a spontaneous magnetization below 230 K, indicating ferro- or ferrimagnetic behavior of Fe_3GeTe_2 (Figure 10, a). The splitting of the zero-field cooled (zfc) and field-cooled (fc) susceptibility measured in an external field of 0.1 T below about 200 K closes for larger external fields (1 and 5 T). We ascribe the splitting of the fc-zfc susceptibilities to irreversible effects due to domain ordering. The inset in Figure 10a displays the magnetization of Fe_3GeTe_2 at 10 K. Saturation is observed for external fields above 5 T with a moment of about 1.2 μ_{Bohr} per Fe atom, about half of the saturated moment of elementary iron.

Ni_3GeTe_2 shows no indication of spontaneous magnetization. Rather, a weak temperature-independent susceptibility is observed above 100 K (Figure 10, b). The increase of the susceptibilities below 50 K can be understood as caused by traces of a paramagnetic impurity, and the field dependence of the susceptibilities as caused by traces of a ferromagnetic impurity.

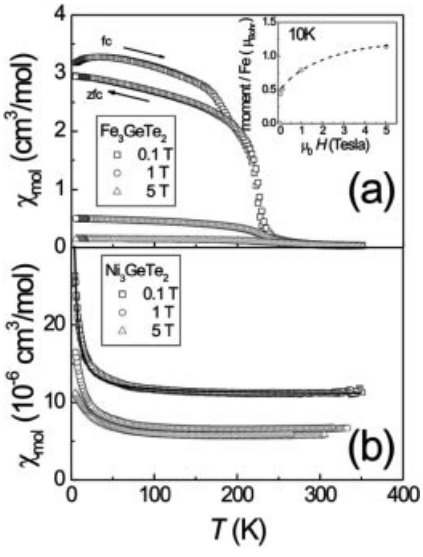

Figure 10. (a) Magnetic susceptibility for Fe_3GeTe_2 as a function of temperature and magnetic field. The inset displays the magnetic moment per Fe atom at 10 K. (b) Magnetic susceptibility for Ni_3GeTe_2 as a function of temperature and magnetic field. The solid line represents a fit of a modified Curie law (see text) to the susceptibility of Ni_3GeTe_2 measured in a field of 0.1 T. The increase in the susceptibility at low temperatures can be ascribed to a temperature-dependent paramagnetic impurity with a concentration of about 0.2% assuming $S = {}^1/_2$ entities with an effective moment of 1.73 μ_B.

The observed field dependence of the magnetic susceptibilities follows if the sample (m = 135 mg) is assumed to contain about 400 μg of elementary ferromagnetic Ni (saturation magnetization 0.62 μ_{Bohr}[14]).

The magnitude and temperature dependence of the electrical resistance (Figure 11) prove Fe_3GeTe_2 is a metal. The magnetic transition shows up as a kinklike anomaly at about 225 K (see inset in Figure 11) because of spin-flip scattering.

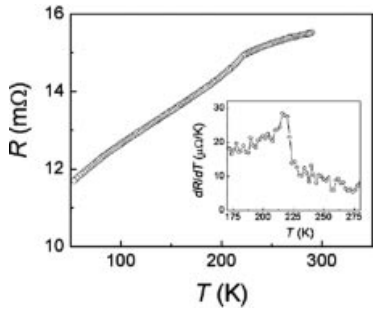

Figure 11. Temperature dependence of the in-plane electrical resistance of a small crystal (approximately $1 \times 1 \times 0.05$ mm^3) of Fe_3GeTe_2. The inset displays the derivative of the in-plane resistance with respect to temperature. A clear maximum of the derivative is seen at the magnetic ordering temperature.

In order to clarify the earlier mentioned valence problems of iron, more detailed magnetic measurements together with Moessbauer investigations are currently in progress.

Experimental Section

Fe_3GeTe_2 was prepared by a direct solid-state reaction starting from an intimate mixture of the pure elements in the molar ratio 3:1:2 (Fe: 99.9%, powder, Heraeus; Ge: 99.99%, powder 250 μm, Chempur; Te: 99.999%, pieces, Chempur). The mixture of the starting materials was filled into a dry quartz glass ampoule, which was evacuated and sealed, heated up to 625 °C, and kept at this temp. for two weeks. The homogeneous gray, air-stable product did not show any impurities in standard X-ray diagrams, melted incongruently at 837 °C, and formed crystals with the shape of small hexagonal plates suitable for X-ray single-crystal experiments. Polycrystalline Ni_3GeTe_2 was prepared in an analogous way (Ni: 99.9%, powder, Heraeus). Bulk material and crystals, viewed under a light microscope, looked very similar to Fe_3GeTe_2, and melted incongruently at 879 °C. However, a more compact and less pronounced layer character of small crystals of the nickel compound became obvious in the scanning electron microscope. Standard powder X-ray diagrams for Ni_3GeTe_2 did not show any contaminations. Further details of the crystal structure investigation for Fe_3GeTe_2 and Ni_3GeTe_2 may be obtained from the Fachinformationszentrum Karlsruhe, 76344 Eggenstein-Leopoldshafen (Germany), on quoting the depository numbers CSD 415616 or CSD 415617, respectively.

For the HRTEM investigations, crystals of Ni_3GeTe_2 were crushed and suspended in *n*-butanol (HRTEM measurements of Fe_3GeTe_2 were not possible because of unexpectedly emerging ferromagnetism already at ambient temp.). One drop of the *n*-butanol suspension was transferred to a perforated carbon/copper net which served as support of the crystallites after drying. HRTEM and SAED investigations were performed with a Philips CM30ST (300 kV, LaB_6 cathode, C_S = 1.15 mm). Computer simulations of the HRTEM images (multislice formalism) and SAED patterns (kinematical approximation) were carried out with the EMS program package[15] (spread of defocus: 70 Å, illumination semiangle: 1.2 mrad). All images were collected with a Multiscan CCD Camera [software Digital Micrograph 3.6.1 (Gatan)]. EDX spectroscopy was performed in the scanning- and nanoprobe mode of CM30ST with a Si/Li-EDX detector (Noran, Vantage System).

Magnetic measurements for both compounds were carried out with the SQUID magnetometer (MPMS, Quantum Design, Dan Diego, USA) of the Max-Planck-Institut für Festkörperforschung (Stuttgart). The in-plane electrical resistance of Fe_3GeTe_2 was measured on a platelet-shaped crystal with dimensions $\approx 1 \times 1 \times 0.05$ mm^3 in the temp. range 50–300 K. Electrical contacts were made by four parallel Cr/Au stripe contacts which had been evaporated on a (110) face of the crystal.

Acknowledgments

The authors would like to thank Mrs. V. Duppel for practical TEM work and Prof. Dr. Dr. h. c. mult. A. Simon for enabling the TEM experiments. The authors are grateful to the "Deutsche Forschungsgemeinschaft" and the "Fonds der Chemischen Industrie" for their financial support.

[1] H. J. Deiseroth, C. Reiner, M. Schlosser, L. Kienle, *Z. Anorg. Allg. Chem.* **2002**, *628*, 1641–1647.
[2] J. Schlirf, H. J. Deiseroth, *Z. Kristallogr.- NCS* **2001**, *216*, 27–28.
[3] N. Kh. Abrikosov, L. A. Bagaeva, LD. Dudkin, L. I. Pertova, V. M. Sokolova, *Izv. Akad. Nauk. SSSR, Neorg. Mater.* **1985**, *21*, 1680.
[4] A. K. Yasukochi, K. Kanematsu, T. Ohoyama, *J. Phys. Soc., Jpn.* **1961**, *16*, 429–433.
[5] M. Ellner, *J. Less-Common Met.* **1976**, *48*, 21–52.
[6] R. L. Abdon, T. Hughbanks, *Angew. Chem.* **1994**, *106*, 2414–2416.
[7] B. Harbrecht, T. Degen, M. Conrad, *J. Alloys Compd.* **1997**, *246*, 37–50.
[8] S. Debus, B. Harbrecht, *Z. Anorg. Allg. Chem.* **2000**, *626*, 173–179.
[9] H.-B. Merker, H. Schäfer, B. Krebs, *Z. Anorg. Allg. Chem.* **1980**, *462*, 49–56.
[10] M. B. Robin, P. Day, *Adv. Inorg. Chem. Radiochem.* **1967**, *10*, 247–422.
[11] S. Furuseth, K. Selte, A. Kjekshus, *Acta Chem. Scand.* **1965**, *19*, 257–258.
[12] G. Brostigen, A. Kjekshus, *Acta Chem. Scand.* **1970**, *24*, 1925–1940.
[13] M. Ellner, T. Goedecke, K. Schubert, *J. Less-Common Met.* **1971**, *24*, 23–400.
[14] D. R. Lide, *CRC Handbook of Chemistry and Physics*, 79th ed., CRC Press, **1998**, pp. 12–117.
[15] P. A. Stadelmann, *Ultramicroscopy* **1987**, *21*, 131–146.

Received: November 16, 2005
Published Online: March 1, 2006

